Available online at www.sciencedirect.com
ScienceDirect
Hydrometallurgy xx (2007) xxx–xxx
hydrometallurgy
www.elsevier.com/locate/hydromet

Determination of the effective thickness of a porous electrode in a flow-through reactor; effect of the specific surface area of stainless steel fibres, used as a porous cathode, during the deposition of Ag(I) ions

J.L. Nava [a,*], M.T. Oropeza [b], C. Ponce de León [c], J. González-García [d], A.J. Frías-Ferrer [d]

[a] Universidad Autónoma Metropolitana-Iztapalapa, Departamento de Química, 55-534, C.P. 09340, México D.F., Mexico
[b] Centro de Graduados e Investigación del Instituto Tecnológico de Tijuana, Blvd. Industrial s/n, CP 22500, Tijuana B.C., Mexico
[c] Electrochemical Engineering Group, Research Institute for Industry, (RIFI), Materials Engineering Group, School of Engineering Sciences, University of Southampton, University Road Highfield, Southampton, SO17 1BJ, United Kingdom
[d] Universidad de Alicante, Departamento de Química Física e Instituto de Electroquímica, Ap. de orreos 99.03080, Alicante, Spain

Received 13 October 2006; received in revised form 22 September 2007; accepted 1 December 2007

Abstract

This study discusses the use of potential distribution analysis during the deposition of metal ions, at limiting current conditions and determines the optimum electrode thickness at which no hydrogen evolution occurs. The potential distribution studies were carried out on stainless-steel fibres of three different surface areas. The fibres were used as cathodic porous electrodes during the deposition of Ag(I) ions contained in 0.1 mol dm^{-3} KNO_3 and 0.6 mol dm^{-3} NH_4OH electrolyte. The comparison between the experimental and the theoretical potential distributions show good agreement at mean linear flow rates in the range of 0.24 and 0.94 cm s^{-1}.

Keywords: Electrode thickness; Flow-through; Fixed bed electrode reactor; Packed bed electrode; Potential distribution; Potential drop; silver ion

1. Introduction

Packed bed electrodes can be used for electrochemical recovery of heavy metals from a variety of industrial and laboratory model solutions (Bennion and Newman, 1972; Doherty et al., 1996; El-Deab et al., 1999; Gaunand et al., 1977; Lanza and Bertazzoli, 2000; Matloz and Newman, 1986; Podlaha and Fenton, 1995; Ponce de León and Pletcher, 1996; Saleh, 2004; Soltan et al., 2003; Trainham and Newman, 1977). The packed bed electrode forms a porous flow-through configuration providing large surface area usually depleting the concentration of metal ions below 0.1 ppm.

Some studies have reported that flow-through configurations suffer from non-uniform potential and current distribution (Bennion and Newman, 1972; Doherty et al., 1996; El-Deab et al., 1999; Gaunand et al., 1977; Matloz and Newman, 1986; Saleh, 2004; Sioda, 1971; Trainham and Newman, 1977). Newman et al. in 1962 demonstrated this problem when Tafel kinetic was coupled with significant solid phase (electrode material) and electrolyte resistivity. In another paper related to the potential and current distribution, Bennion and Newman (1972) used the deposition of copper ions on carbon flakes to study the design principles of flow-through porous electrodes. The authors concluded that flow rate and bed thickness determine the ohmic potential drop within the porous electrode. Another conclusion was that the potential difference between the carbon matrix and the solution at all points within the porous electrode should be sufficient, but not too large to ensure deposition without hydrogen evolution. Sabacky and Evans (1979) used a fluidised copper particles cathode for copper recovery and reported that the efficiency and power consumption depended on copper and acid concentration, particle size, resistivity of the electrolyte and superficial current density. Their model predicted inefficient utilization of the bed surface

* Corresponding author. Tel.: +52 55 5804 4600x2685; fax: +52 55 5804 4666.
E-mail address: jlnm@xanum.uam.mx (J.L. Nava).

0304-386X/$ - see front matter © 2007 Elsevier B.V. All rights reserved.
doi:10.1016/j.hydromet.2007.12.001

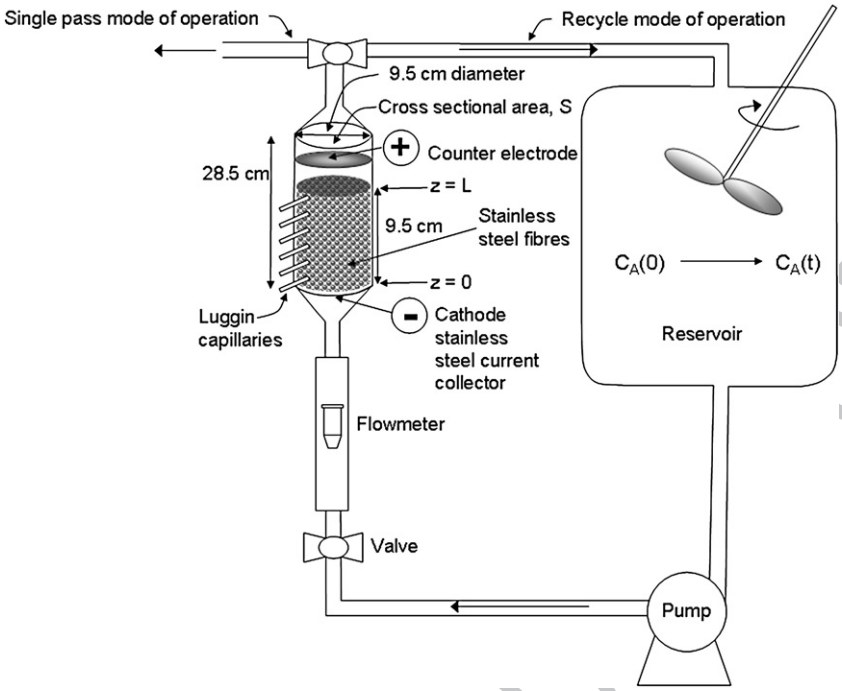

Fig. 1. Experimental flow circuit and packed bed electrochemical reactor.

area at high values of electrode and electrolyte resistivity and introduced the effectiveness factor to compare maximum and actual limiting currents. The influence of electrolyte and electrode resistivity turned to be small when compared with the bed resistivity originated by the bed expansion caused by hydrogen bubbles at high cathode voltages. In a more recent paper, Saleh in 2004 re-introduced the concept of effectiveness factor as the ratio between the total obtainable limiting current and the maximum limiting current in absence of ohmic drop. The study was based on the deposition of zinc in alkaline solution where the hydrogen evolution reaction and the deposition of zinc take place at similar potential. Saleh concluded that hydrogen evolution accentuates the ohmic effect. Similarly, Like and Langer in 1991 discussed the internal ohmic limits in a flow-through porous electrode using Tafel kinetics. They showed that during the electrolyses, thinner electrodes help to maximize the current density.

The aim of this paper is to use a potential distribution analysis to estimate the optimum length of a packed bed electrode reactor during a metal recovery process avoiding secondary reactions such as the hydrogen evolution. This is shown by taking the deposition of Ag(I) ions on three stainless steel fibres porous cathodes of different specific surface areas. The potential region for the reduction of Ag(I) ions at mass transport controlled conditions was determined by rotating disc electrode experiments (RDE). A potential value in this region was then selected for the electrolysis experiments in a flow cell. Mass transport characterization of the three stainless steel fibres porous electrodes was used to obtain the parameters included into the one-dimension potential distribution model. The theoretical potential distribution calculations were compared with the experimental data.

2. Mass balance in a recirculating flow-through reactor with 3D electrode

The concentration profile of the electroactive species in a flow-through reactor in batch recycle mode of operation (see Fig. 1), neglecting phase changes and dispersion effects in the porous electrode, can be described by the following equation (Fahidy, 1985):

$$\frac{C(t)}{C(t=0)} = \exp - \left[\frac{t}{\tau_T}\left(1 - \exp^{-[\alpha L]}\right)\right] \quad (1)$$

where $C(t)$ and $C(t=0)$ are the concentration of the electroactive species during the electrolysis at time t and 0 respectively, τ_T is the mean residence time of the electrolyte in the reservoir defined as $\tau_T = V_T/Q$, where V_T and Q are the volume of the reservoir and the volumetric flow rate. L is the length of the porous electrode and α is the following group parameter:

$$\alpha = \frac{k_m a(1-\varepsilon)}{u} \quad (2)$$

where k_m is the average mass transport coefficient assuming that it is independent of the axial position (z), a, is the specific surface electrode area, is the electrode porosity and u is the mean linear flow velocity of the electrolyte.

3. Potential distribution in a single pass flow-through reactor with 3D electrode

The unidirectional potential distribution in electrically conductive porous electrodes under limiting current conditions can

Please cite this article as: Nava, J.L., et al., Determination of the effective thickness of a porous electrode in a flow-through reactor; effect of the specific surface area of stainless steel fibres, used as a porous cathode, during the deposition of Ag(I) ions, Hydrometallurgy (2007), doi:10.1016/j.hydromet.2007.12.001

Table 1
Physical properties of the three stainless-steel fibres porous electrode of 2.9 g cm^{-3} density contained in reactor of 71 cm^{-2} cross sectional area and 9.5 cm long

Specific surface area*	Porosity	Electrode area per gram
a/cm^{-1}	/ε	/cm^2 g^{-1}
193	0.969	66
107	0.910	37
81	0.907	286

*The specific surface area of the porous electrode, a, (geometric area of the electrode/volume occupied by the electrode) was calculated by multiplication of the electrode area per gram by the electrode density.

be modelled by assuming plug-flow conditions and neglecting conductivity changes of the electrolyte during electrolysis due to an excess of supporting electrolyte. The model assumes that only the concentration decay of the electroactive species within the electrode is responsible for the potential distribution (Fahidy, 1985):

$$\varphi_e(z) - \varphi_e(z=0) = -\frac{\mathrm{nFuC}(z=0)}{\alpha\sigma_e}\left[\alpha z + \exp^{-\alpha z} - 1\right] \qquad (3)$$

where $\varphi_e(z)$ is the potential of the electrolyte at any position within the interstitial spaces of the electrode, $\varphi_e(z=0)$ is the potential at the inlet of the electrode, n is the number of electrons transferred, F the Faraday constant, $C(z=0)$ is the concentration of the electroactive species at the inlet of the porous electrode, and σ_e is the conductivity of the electrolyte in the interstitial space of the porous electrode given by (Fahidy, 1985):

$$\sigma_e = \sigma\frac{2\varepsilon}{(3-\varepsilon)} \qquad (4)$$

where σ is the conductivity of the electrolyte.

4. Experimental

4.1. Equipment and solutions

The electrolyte consisted of 4.6×10^{-3} mol dm^{-3} $AgNO_3$, 0.1 mol dm^{-3} KNO_3 and 0.6 mol dm^{-3} NH_4OH (Oropeza et al., 1995) and was prepared using analytical grade reactants dissolved in deionised water (Milli-Q™). This solution was used for both the RDE and the flow cell experiments. In the flow cell, 5 L of this solution were circulated through the electrolyte circuit (Fig. 1). A potentiostat–galvanostat PAR™ Model 273A was used to apply and control the potential of both the RDE and the stainless steel porous electrodes. All potentials are referred to the standard hydrogen electrode, SHE. The solutions were deoxygenated during approximately 10 min and the experiments were carried out under a nitrogen atmosphere at 25±3 °C.

4.2. Electrochemical cells

4.2.1. Experiments at the rotating disc electrode (RDE) cell

A three glass electrode electrochemical cell of 100 mL capacity with nitrogen inlet was used. A Tacussel™ rotating disk electrode assembly model F69100 was used with this cell. The working electrode was stainless steel disk of 0.0314 cm^{-2} and the reference and counter electrodes were saturated sulphate (SSE) (Tacussel™ model XR200) and a graphite bar, respectively. The working electrode was polished with 0.3 μm alumina powder followed by 5 min of ultrasonic bath and a final rinse with distilled water before each experiment. The ultrasonic bath helps to remove the traces of alumina left on the electrode surface.

4.2.2. Experiments in the packed bed flow cell

Fig. 1 shows a schematic diagram of the packed bed flow cell; the body of the reactor consists of a propylene tube of 28.5 cm length and 9.5 cm internal diameter. The tube was fitted with flanges at both ends. Two Nylon cones with a flange were attached at the top and bottom of the tube using the flanges in order to form the inlet and outlet of the reactor. The conical shape improves the distribution of the fluid at the inlet and avoids back mixing of the electrolyte at the exit. The polypropylene tube contained stainless steel 304 fibres as a cathode electrode. Three different specific surface area fibres supported by a stainless steel mesh current collector of 9.4 cm diameter were used separately as porous electrodes. The fibres were obtained by changing the distance between the cutting tool and a stainless steel rod mounted on a lathe. The specific area of the packed bed electrode was calculated by multiplying the electrode area per gram (cm^2 g^{-1}) by its density; Table 1 shows the parameters of this material. Small plastic tubes inserted on 3 mm holes drilled along the propylene tube length were used as Luggin capillaries to monitor the local potential of the solution throughout the packed bed electrode (see Fig. 1). A titanium mesh covered with a layer of RuO_2 was used as counter electrode at the top of the reactor.

A March MFG pump of 1/25 hp was used to recirculate the electrolyte through the reactor and the flow rates were measured using a variable area polycarbonate flowmeter (Cole Palmer model F44376LH-8). The electrolyte flow circuit was constructed with Master Flex tubing, (C-Flex 6424-16, 0.5 in. diameter). All the valves and three way connectors were assembled with PVC materials. The electrolyte was contained in a 5 litre reservoir fitted with a stainless-steel stirrer powered by a 115 V Caframo™ electric motor of variable velocity used to achieve well mixed conditions. The electrolyte circuit was designed to allow single pass or recirculation modes of operation.

During electrolysis, the concentration of silver ions was potentiometrically determined using an ion selective electrode (ISE) model 9616N from Orion Research Inc.™. The electrode was calibrated each time a new sets of samples from a different experiment were taken and was allowed to equilibrate with solutions of similar concentration of Ag(I) ions expected from the samples. The potential of the electrolyte along the packed bed working electrode was monitored with a saturated sulphate reference electrode SSE (E=615 mV *vs.* SHE), connected to the Luggin capillaries.

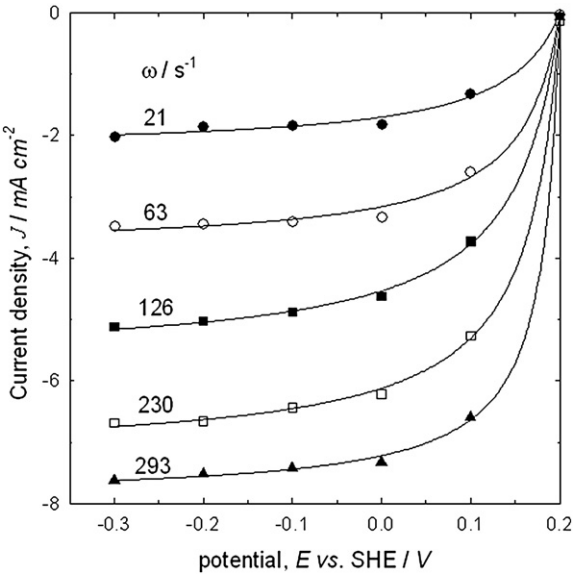

Fig. 2. Current density *vs.* potential curves for Ag(I) ions deposition process. Electrolyte: 4.6×10^{-3} mol dm^{-3} $AgNO_3$ in 0.1 mol dm^{-3} KNO_3 and 0.6 mol dm^{-3} NH_4OH.

Please cite this article as: Nava, J.L., et al., Determination of the effective thickness of a porous electrode in a flow-through reactor; effect of the specific surface area of stainless steel fibres, used as a porous cathode, during the deposition of Ag(I) ions, Hydrometallurgy (2007), doi:10.1016/j.hydromet.2007.12.001

5. Analysis of results and discussion

5.1. Determination of electrolysis potential for Ag(I)/Ag(0) reduction process

Current *vs*. time curves were recorded with different potential steps applied to the stainless steel rotating disc electrode. The potential steps were from the open circuit potential (OCP) at 0.2 V *vs.* SHE to 0.1, 0.0, −0.1, −0.2 and −0.3 V *vs.* SHE each at different angular velocities. The deposited silver was stripped off from the electrode by applying a positive potential of 0.35 *vs.* SHE after each chronoamperometric experiment, followed by the polishing procedure outlined in the experimental section. These chronoamperometric plots were used to construct the current density *vs*. potential curves for Ag(I) ion deposition taking the current at time *t*, of 6 s after the potential step was applied. Fig. 2 shows the current density *vs.* potential curves obtained from the chronoamperometric experiments at different angular velocities and shows that metallic silver deposition starts at less than 0.2 V *vs*. SHE for all rotation rates with the limiting current plateau between 0.0 V and −0.3 V *vs.* SHE. Although not shown in the Figure it was observed that hydrogen evolution started at <−0.3 V *vs*. SHE.

The RDE experiments established that silver ion deposition was mass transport controlled between 0.0 V and −0.3 V *vs*. SHE. It is important to point out that even when the limiting current plateau started slightly positive to 0 V *vs*. SHE in the RDE for all angular velocities (see Fig. 2) the potential value used for the electrolysis in the flow-through electrode was +0.1 V *vs*. SHE applied at $z=0$ (see Fig. 1). The assumption is that at such potential the process is still mass transport controlled in the packed bed electrode system.

5.2. Mass transport characterization in the packed bed electrode.

The mass transport coefficients were determined by electrolysis of Ag(I) ion solutions in the packed bed flow-through reactor in recycle mode of operation (Fig. 1). The electrolysis were carried out by applying +0.1 V *vs.* SHE on the current collector, at $z=0$, situated at the inlet of the packed bed electrode reactor. Since it is unlikely that the RDE and the packed bed cell developed the same mass transport, the selection of the electrolysis potential was based on the fact that the average mass transport in the packed bed electrode is lower than in the rotating disc electrode. The calculation of the mass transport coefficient in the RDE and in the packed bed systems was 9×10^{-3} cm s^{-1} and 7×10^{-4} cm s^{-1} respectively, showing that k_m is approximately one order of magnitude larger in the RDE cell. This justifies the selection of +0.1 V *vs.* AgCl for mass transport controlled electrolysis in the packed bed electrode. The mean linear flow velocities, u, during the electrolysis, were between 0.23 and 0.94 cm s^{-1}.

Table 2
Properties and parameters used to model the potential distribution throughout the packed bed electrode

Concentration of Ag(I) at the entrance of porous electrode	Electrolyte conductivity	Electrons transferred
$C(z=0)$/mol cm^{-3} X 10^6	σ/Ω^{-1} cm^{-1}	n
4.6	0.100	1

Fig. 3 shows the mean mass transport coefficients multiplied by the electrode area k_ma, *vs*. the mean linear flow velocity u, for the three packed bed electrodes. These values were obtained from the slopes of the curves of concentration decay *vs*. time during the electrolysis of Ag (I) ions and applying the Eq. (1). The mass transport coefficients increased with the specific surface area of each electrode and with the mean linear flow velocity of the electrolyte. From the correlations $k_ma=bu^c$ showed in the plots, it can be observed that in the three electrodes of different specific surface area, the value of the velocity exponent, c, falls between 0.55 and 0.95, indicating that the flow pattern is a complex function of the specific surface area, electrode porosity and shape of the fibres (Delanghe et al., 1990; Langlois and Coeuret, 1989). On the other hand, the values of the coefficient b, associated with the electrode geometry, increased with the specific surface area showing the interdependence of this parameter in the mass transport correlation. It is important to mention that the exact form of

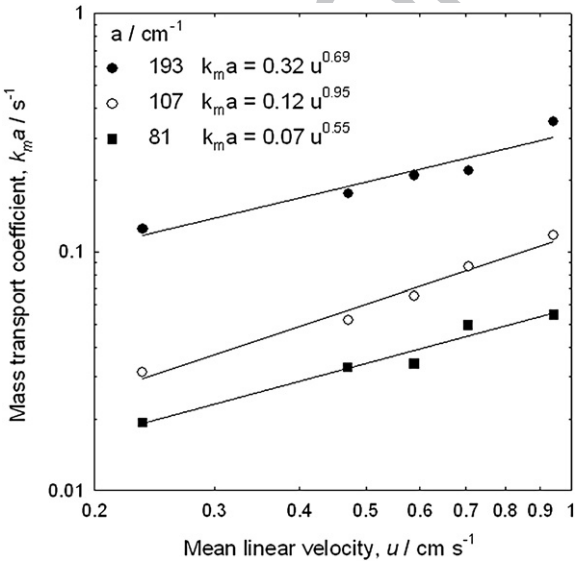

Fig. 3. Mass transport coefficients *vs*. mean linear flow electrolyte velocity for the reduction of Ag(I) ions. Specific areas of stainless-steel fibres: 81, 107 and 193 cm^{-1}. Potential of the electrolysis at $z=0$: 0.1 V *vs*. SHE.

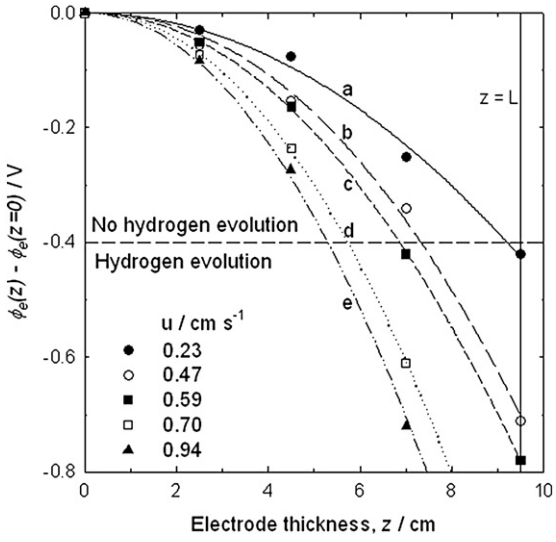

Fig. 4. Comparison between experimental and theoretical potential distribution in the packed bed electrode reactor during the deposition of Ag(I) ions. The lines represent the theoretical approach (Eq. (10)); a) 0.23, b) 0.47, c) 0.59, d) 0.70 and e) 0.94 cm s^{-1}. The symbols are the values obtained experimentally. Working electrode: stainless steel-fibre of 81 cm^{-1} specific surface area. Potential of the electrolysis at $z=0$: 0.1 V *vs*. SHE.

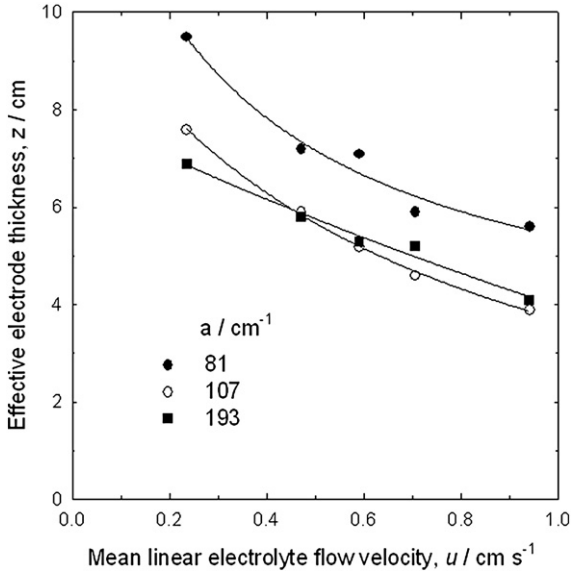

Fig. 5. Effective electrode thickness vs. mean linear flow velocity for the reduction of Ag(I) ions on three different specific surface area packed bed electrodes. The lines show the position on the electrode height, z, before hydrogen evolution starts, i.e. for potential drop $\varphi_e(z)-\varphi_e(z=0)\leq -0.400$ V. Working electrodes: stainless-steel fibres.

the mass transport correlation is best evaluated through analysis of experimental data because it depends on the geometry of the electrode, type of fluid flow pattern, and the electrochemical reaction (Delanghe et al., 1990). In the following section the potential distribution curves are simulated using the $k_m a$ values from Fig. 3.

5.3. Potential distribution in the packed bed electrode; determination of the effective cathode thickness

The experimental measurements of the potential distribution were carried during the electrolysis of Ag(I) ions in the flow-through reactor in a single pass mode of operation (Fig. 1). The electrolysis were carried out by applying 0.1 V *vs.* SHE on the current collector, at $z=0$, situated at the inlet of the packed bed electrode reactor. The maximum potential drop before hydrogen evolution starts, will be: $\varphi_e(z)-\varphi_e(0)=-0.3-0.1=-0.4$ V. This allows a potential window of 0.4 V between the deposition of Ag(I) ions and the beginning of the hydrogen evolution reaction. This criterion, supported by current density *vs.* potential curves (Fig. 2), was previously proposed by Kreysa et al. (1971) to estimate the thickness of a porous electrode. The experimental potential distribution was compared to that obtained theoretically by using Eq. (3) and the data is shown in Tables 1 and 2.

Fig. 4 shows both, the experimental (symbols) and theoretical (lines) variation of the axial potential distribution with the position of the electrode z, at several mean linear velocities of the electrolyte, u, for a 81 cm^{-1} specific surface area electrode. This Figure shows that there is a good agreement between the experimental and theoretical values over the length of the electrode. The potential becomes more negative as z increases due to the concentration decay of the electroactive species (Bennion and Newman, 1972; Fahidy, 1985; Newman and Tobias, 1962; Sioda, 1971).

The potential difference observed at a mean linear flow velocity of 0.23 cm s^{-1} (Fig. 4), shows that hydrogen evolution will occur only when $z>9.0$ cm length, since $(\varphi_e(z)-\varphi_e(z=0))<-0.400$ V at this length. At higher mean linear flow velocities, the curves indicate that hydrogen evolution will start at lower electrode lengths, as $\varphi_e(z)-\varphi_e(z=0)<-0.400$ V. For example at mean linear flow velocities of 0.47, 0.59, 0.70 and 0.94 cm s^{-1} the evolution of hydrogen begins at z equal to 7.3, 6.8, 5.8 and 5.3 cm, respectively. This is shown in Fig. 4 when the lines that represent the potential intersect the horizontal line at −0.4 V *vs.* SHE that defines the beginning of the hydrogen evolution reaction.

In order to show the maximum permissible length along the axial axis of the electrode at which no hydrogen evolution occurs, i.e. where $\varphi_e(z)-\varphi_e(z=0)=-0.400$ V, the electrode length z was plotted *vs.* the mean linear flow velocity u, for the 81, 107 and 193 cm^{-1} specific surface area packed bed electrodes in Fig. 5. These data show the effective electrode thickness before hydrogen evolution starts. In the three cases, the maximum electrode length is shorter as the mean linear flow velocity increases however, the maximum permissible length at which no hydrogen evolution occurs is larger for the 81 cm^{-1} specific surface area electrode at all velocities. The points of effective electrode thickness for 107 and 193 cm^{-1} specific surface area at different mean linear velocities behave similarly.

The larger permissible lengths obtained for the 81 cm^{-1} specific surface area electrode are due to the fact that on this electrode the concentration decay of the electroactive species is less rapid than on electrodes with higher specific surface area. Nevertheless for design purposes, the evolution of hydrogen should be avoided by adjustment of the values of the mean linear flow velocity and the specific surface area for a fixed electrode length.

The potential distribution results show the usefulness of this type of analysis to estimate the optimum length of a packed bed electrode reactor which allows efficient recovery of metals by avoiding hydrogen evolution.

6. Conclusions

This work showed the use of potential distribution studies in the design of a bed thickness of a flow-through porous electrode during deposition of Ag(I) ions in KNO_3+NH_4OH aqueous electrolyte. The comparison of both, experimental and theoretical potential distributions showed that flow rate and specific surface area of the electrode determine the potential drop within the packed bed cathode and therefore the effective thickness of the porous bed electrode at which hydrogen evolution can be avoided. The method used in this paper can be applied to other electrically conductive flow-through porous electrode shapes to establish the optimum electrode thickness.

7. Uncited reference

Q3

Walker and Wragg, 1977

References

Bennion, D.N., Newman, J., 1972. Electrochemical removal of copper ions from very dilute solutions. J. Appl. Electrochem. 2, 113–122.

Delanghe, B., Tellier, S., Astruc, M., 1990. Mass transfer to a carbon or graphite felt electrode. Electrochim. Acta 35, 1369–1376.

Doherty, T., Sunderland, J.G., Roberts, E.P.L., Pickett, D.J., 1996. An improved model of potential and current distribution within a flow-through porous electrode. Electrochim. Acta 41 (4), 519–526.

El-Deab, M.S., Saleh, M.M., El-Anoduli, B.E., Ateya, B.G., 1999. Electrochemical removal of lead ions from flowing electrolytes using packed bed electrodes. J. Electrochem. Soc. 146 (1), 208–213.

Fahidy, T.Z., 1985. Principles of Electrochemical Reactors Analysis. Elsevier, pp. 221–223.

Please cite this article as: Nava, J.L., et al., Determination of the effective thickness of a porous electrode in a flow-through reactor; effect of the specific surface area of stainless steel fibres, used as a porous cathode, during the deposition of Ag(I) ions, Hydrometallurgy (2007), doi:10.1016/j.hydromet.2007.12.001

Gaunand, A., Hutin, D., Coeuret, F., 1977. Potential distribution in flow through porous electrodes under limiting current conditions. Electrochim. Acta 22 (1), 93–97.

Langlois, S., Coeuret, F., 1989. Flow-through and flow-by porous electrodes of nickel foam. II. Diffusion-convective mass transfer between the electrolyte and the foam. J. Appl. Electrochem. 19, 51–60.

Lanza, M.R.V., Bertazzoli, R., 2000. Renoval of Zn(II) from chloride médium using a porous electrode: current penetration withing the cathode. J. Appl. Electrochem. 30 (1), 61–70.

Like, S.E., Langer, S.H., 1991. Internal ohmic drop limits on effectiveness of packed bed electrodes obeying Tafel kinetics. J. Electrochem. Soc. 138, 2327–2330.

Matloz, M.J., Newman, J., 1986. Experimental investigation of a porous carbon electrode for the removal of mercury from contaminated brine. J. Electrochem. Soc. 133 (9), 1850–1859.

Newman, J., Tobias, C.W., 1962. Theoretical analysis of current distribution in porous electrodes. J. Electrochem. Soc. 109, 1183–1191.

Oropeza, M.T., González, I., Palomar, M., 1995. Patent No. 9101212, México.

Podlaha, E.J., Fenton, J.M., 1995. Characterization of a flow-by RVC electrode reactor for the removal of heavy metals from dilute solutions. J. Appl. Electrochem. 25, 299–306.

Ponce de León, C., Pletcher, D., 1996. The removal of Pb(II) from aqueous solutions using a reticulated vitreous carbon cathode cell—the influence of the electrolyte medium. Electrochim. Acta 41 (4), 533–541.

Sabacky, B.J., Evans, J.W., 1979. Eectrodeposition of metals in fluidized bed electrodes Part I. Mathematical model. J. Electrochem. Soc. 126, 1176–1180.

Saleh, M.M., 2004. On the effectiveness factor of flow-through porous electrode. J. Phys. Chem., B 108, 13419–13426.

Sioda, R.E., 1971. Distribution of potential in a porous electrode under conditions of flow electrolysis. Electrochim. Acta 16, 1569–1576.

Soltan, E.A., Nosier, S.A., Salem, A.Y., Mansour, I.A.S., Sedahmed, G.H., 2003. Mass transfer behaviour of a flow-by fixed bed electrochemical reactor under different hydrodynamic conditions. Chem. Eng. J. 91, 33–44.

Trainham, J.M., Newman, J., 1977. A flow through porous electrode model: application to metal ion removal from dilute streams. J. Electrochem. Soc. 124 (10), 1528–1540.

Walker, A.T.S., Wragg, A.A., 1977. The modelling of concentration-time relationships in recirculating electrochemical reactor systems. Electrochim. Acta 22, 1129–1134.

List of symbols

Symbol: Meaning

A: Specific surface area of the porous electrode (geometric area/volume of the electrode) (cm^2/cm^{-3})

B: Constant (Dimensionless)

C: Constant (Dimensionless)

C(z=0): Concentration of electroactive species at the point of $z=0$ of the porous electrode (mol cm^{-3})

C(t): Concentration of the electroactive species in the reservoir at any time, t (mol cm^{-3})

C(t=0): Concentration of the electroactive species in the reservoir at time $t=0$ (mol cm^{-3})

dp: Particle size, shown in Table 1 (cm)

E: Potential (V)

k_m: Average mass transport coefficient (cm s^{-1})

F: Faraday constant, 96,485 (C mol^{-1})

J: Current density (A cm^{-2})

L: Electrode height, 9.5 cm

n: number of electrons transferred (dimensionless)

Q: Volumetric flow rate (cm^3 s^{-1})

t: Time of electrolysis (s)

u: Mean linear electrolyte velocity in empty channel (cm s^{-1})

V_T: Volume occupied by the electrolyte in the reservoir (cm^3)

z: Any arbitrary point along the porous electrode (cm)

Greek symbols

Symbol: Meaning

α: Parameter group, $\frac{k_m a(1-\varepsilon)}{u}$ (cm^{-1})

ε: Electrode porosity (Dimensionless)

$(1-\varepsilon)$: Fraction occupied by the porous electrode (Dimensionless)

$\varphi(z)$: Potential difference at any position along the electrode (V)

$\varphi_e(z)$: Electrolyte potential in an arbitrary position (V)

$\varphi_e(z=0)$: Electrolyte potential at the packed electrode inlet (V)

φ_M: Potential in the matrix of bed electrode (V)

σ: Electrolyte conductivity (Ω^{-1} cm^{-1})

σ_e: Interstitial conductivity, $\sigma_e = \sigma\frac{2\varepsilon}{(3-\varepsilon)}$ (Ω^{-1} cm^{-1})[1]

τ_T: Residence time of the electrolyte in the reservoir, $\tau_T = \frac{V_T}{Q}$ (s)

ω: Angular velocity (s^{-1})

Please cite this article as: Nava, J.L., et al., Determination of the effective thickness of a porous electrode in a flow-through reactor; effect of the specific surface area of stainless steel fibres, used as a porous cathode, during the deposition of Ag(I) ions, Hydrometallurgy (2007), doi:10.1016/j.hydromet.2007.12.001